

Pulsars and their Surrounding Nebulae: Energy Transfer Calculations and Data Analysis in Python

Department of Physics, University of California, Santa Barbara, CA 93106

December 5, 2022

Abstract

This paper will cover the topic of Pulsars and their energy dissipation, in relation to both magnetic and electromagnetic fields. This study aims to correlate the energy losses of Pulsars to the luminosity of the Pulsar Wind Nebulae that surround them. One example calculation will be carried out in detail while the data gathered will be analysed in Python, from which we draw our results.

1 Introduction

Although Pulsars and their specifics are still not fully understood, we understand enough to describe how they interact with their surroundings. This includes, but is not limited to, the surrounding Supernova Remnants (SNR), Pulsar Wind Nebulae (PWNe), or a combination of both. This introduction will serve to describe the curious phenomena of Pulsars and their surrounding PWNe and offer scientific – as well as historical – context and significance. We omit the discussion of the initial ejecta left behind from the supernova, as it is not central to the topic at hand. Furthermore, for the Pulsar and PWN expert, this section can be skipped without loss of continuity or generality.

1.1 Pulsars

1.1.1 Physical Properties

As the life of a very massive star – over eight times the mass of our sun – comes to an end, its core starts to collapse inwards and its outer layers expand outwards. At the point when there is no more fuel left for the star to burn, the outwards pressure gradient sustaining and counterbalancing the self gravity of the celestial body disappears, and the outer layers implode onto the now extremely dense core. Layers upon layers of solar masses collide

with a now extremely dense core and the result is an extremely powerful explosion, what we call a supernova, that ejects material radially outwards from where the star used to be.

While all of this is occurring, the former core of the star, which was rotating at a slow rate due to magnetic fields and conservation of angular momentum, now begins to rotate faster and faster. This is really just elementary mechanics: as the diameter of the spinning body decreases, the angular velocity increases. After all is said and done, the result is supernova ejecta being flung into space and a rapidly rotating, extremely dense body that's left behind.

The mass of this object is so extreme that the self gravity begins the process of neutron formation, combining protons and electrons to create neutrons, with neutrinos ejected into space as a byproduct:



Now, the rapidly rotating body is composed almost entirely of neutrons, and the self gravity is so extreme, neutron degeneracy pressure is the only mechanism to support it. The density of this body is the most extreme known to exist in the universe: we call it a neutron star, and is second densest only to a black hole.

A pulsar is simply a rapidly rotating neutron star that has its rotation axis unaligned with its magnetic axis.

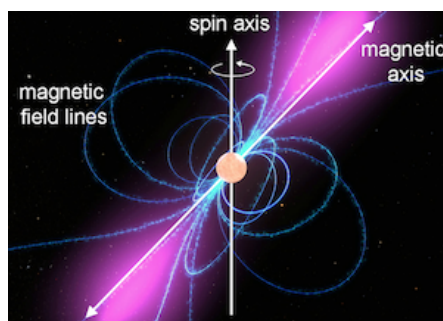


Fig. 1: The difference between the spin axis and magnetic axis of a pulsar produce the 'lighthouse effect' distinctive of a pulsar.

This spinning "magnet" of sorts generates an enormous magnetic field and ejects particles outwards from its magnetic poles, sweeping the cosmos with these "beams" of electromagnetic radiation. (Really, any rotating neutron star is a pulsar, but its frequency of pulsation is not noticeable if the two axes – rotation and magnetic – are aligned.)

1.1.2 Relevant equations

A neutron star of mass M and radius R rotates at an angular velocity $\Omega = \frac{2\pi}{P}$, where P is the period of one full revolution. Since the rotating body is in equilibrium – the self-gravitational acceleration equals its centripetal acceleration – the density can be modeled as

$$\rho > \frac{3\pi}{GP^2}, \quad (2)$$

and displays just how dense these objects can become if the period is plugged in to the equation.

Furthermore, a star's core that is more massive than the Chandrasekhar Mass¹ cannot be supported by electron degeneracy pressure and collapses into a neutron star, as described above. Therefore, as a function of period P and mass M , a maximum radius R is defined:

$$R < \left(\frac{GMP^2}{4\pi^2} \right)^{\frac{1}{3}}. \quad (3)$$

In the process of core collapse of a star, the magnetic flux

$$\Phi \equiv \int \vec{B} \cdot d\vec{a} \quad (4)$$

through its surface is maintained constant, while its surface area shrinks to billions of times as small, resulting in a drastic increase of its magnetic field. The result is an extremely powerful magnetic dipole, which if tilted at an angle from its rotation axis, releases large amounts of magnetic radiation governed by

$$P_{rad} = \frac{2}{3c^3} (BR^3 \sin \alpha)^2 \left(\frac{2\pi}{P} \right)^4 \quad (5)$$

where c is speed of light, B is magnetic field, R is radius, α is inclination angle, and P is period of rotation. This radiation feeds directly into the surrounding nebula, powering it up.

The pulsar, due to its rotation, has rotational kinetic energy

$$E = \frac{I\Omega^2}{2} = \frac{2\pi^2 I}{P^2} \quad (6)$$

with I its moment of inertia. As magnetic dipole radiation emits energy, and its moment of inertia remains constant, a loss of angular velocity occurs. We define

$$\dot{P} \equiv \frac{dP}{dt} > 0 \quad (7)$$

as the spin down rate.

Now, finally, we can define a spin down luminosity, or energy loss due to rotation which we presume to equal the luminosity of dipole radiation:

$$-\dot{E} = -I\Omega\dot{\Omega} = \frac{4\pi^2 I \dot{P}}{P^3} \quad (8)$$

1.1.3 Discovery and Current Findings

After spending two years constructing a radio telescope while doing her Ph.D. at Cambridge, Jocelyn Bell noticed strange signals coming from one specific point in the night sky. Bell, and her supervising professor

¹Around 1.4 Solar masses.

Hewish, ruled out all sources of possible interference, and decided to jokingly call it "Little Green Men" (LGM-1). They were unsure what to label their findings, but after noticing the same phenomena multiple times from various parts of the night sky, they realized they had discovered a new type of phenomenon in the cosmos: the pulsar.

In the years that have passed, thousands of Pulsars have been located in the universe, from a multitude of radio and high-energy telescopes and surveys from around the globe. Some notable ones – and important ones for our research – include the Australian National Telescope Facility (ATNF) and the High Energy Spectroscopic System (H.E.S.S.) survey.

The ATNF is managed by Australia's national science agency CSIRO and includes many different telescopes in various locations, offering a vast view of the radio spectrum of the southern hemisphere. A few of their major facilities include the Murchinson radio observatory and the Parkes radio telescope, the latter of which we use extensively for our data collection in this paper. The ATNF aims to provide state of the art radio telescopes for the CSIRO and the whole planet for the continued discovery of phenomena in the observable universe.

H.E.S.S was an almost ten year long survey conducted using gamma-ray telescopes in Namibia with the goal of discovering high energy objects in the night sky. Over 70 objects were found in the galactic plane, of which tens are pulsars, PWNe, and SNR. The observing of such phenomena in the gamma-ray part of the spectrum leads to important discoveries of the fundamental mechanisms of pulsars and their nebulae, of which we use in our paper to correlate the two.

1.2 Pulsar Wind Nebulae

As a pulsar spins, it not only generates a lighthouse effect of radio and x-ray beams from its poles but also generates a strong wind of charged particles such as positrons and electrons that interact with the surrounding gas. These charged particles collide with the surrounding nebula and give off light over the entirety of the electromagnetic spectrum.

As mentioned before, the H.E.S.S. survey has located many tens of PWNe, and offers data on their luminosities in various bands that we make use of here in this paper. While we do use the H.E.S.S. collected data, we are not limited to just those in this paper.

1.3 Interaction

Having introduced the physical makeups of both pulsars and pulsar wind nebulae, we are ready to tackle the essential question of how and why the two are related. The physics is very clear and the math never lies: pulsars do slow down over time and that energy loss should be accounted for in the observable luminosity – in all bands – of the nebula that surrounds it. Many papers prior to this one have set out to answer the same question, and with varying methods and data. The general accepted consensus in the scientific community is that indeed pulsar rotational spin down luminosity can be directly accounted for in the luminosity of the surrounding PWN.

We aim to reproduce their results with one example calculation and with rigorous statistical analysis of the supposed linear relationship these phenomenons are related by in their energy transfer. We gather data from a variety of sources and check our calculated results with those of prior research papers.

2 Methods

2.1 Luminosity Calculation

We begin our discussion of the relation of pulsar spin down energy loss with the surrounding pulsar wind nebula luminosity with an example calculation. The aim here is to put to use the various equations governing the behavior of pulsars and the process of deriving luminosity from an image of the pulsar wind nebula in question.

For this example, we chose to derive the energy of the Crab Pulsar and surrounding Crab Nebula. Since the Crab Pulsar is very well studied and can be considered very similar to the 'canonical' pulsar, it is the perfect candidate. The pulsars parameters – specifically it's spin frequency rate of change of spin frequency – can be readily accessed. The quantity \dot{E} can be easily derived using Eq. 8 above.

The Crab Nebula – also named M1 in the Messier catalogue – is the surrounding pulsar wind nebula we wish to derive the luminosity of. We chose to utilize the resources available to us in the Las Cumbres Observatory (LCO) telescopes. The LCO is a global telescope network which spans 6 of the 7 continents and provides access to its network of telescopes for other institutions or researchers across the world. For the calculations we carried out, we requested images from the LCO. They captured images of the Crab Nebula for us using one of their 0.4 meter telescopes in Tenerife, one of the Canary Islands. The telescope uses a SBIG STL6303 sensor, and the many other specifications can be found on their website.

As requested, 20 images were taken total; 10 frames of the Crab Nebula in the Bessel B filter, and 10 in the Bessel V. These filters were chosen because of the available reference star data. Other filters such as SDSS filters were also available for our use, but the related reference star data were not readily accessible.

We begin our calculation by aligning, stacking and averaging the 10 frames in one filter of the pulsar wind nebula. The software used to conduct these operations is AstroArt, an astronomical image processing software². Using the integrated tools, background flux can be subtracted off from the total flux on the array of pixels in the image to reduce the signal to noise ratio of the image and produce science frames to be used for analysis. Now, armed with the given magnitude for this specific bandpass of the reference star HD254 – 010, the fluxes of both the reference star and the Crab nebula, we calculate the relative magnitude of the Crab Nebula:

$$m_{M1} - m_{Star} = \ln(F_{M1}/F_{Star}). \quad (9)$$

²More information can be found on their website: <https://www.msb-astroart.com/>

Now, we can compute the absolute magnitude of the Crab Nebula. The equation

$$M = m + 5 - 5 * \log_{10}(distance) \quad (10)$$

allows for the calculation of the absolute magnitude from the relative one found prior. The flux needed for the magnitude found for the specific band pass can be found here. Now, we can find the flux, and using the equation

$$\frac{F_1}{F_2} = 10^{0.4*(M_2 - M_1)} \quad (11)$$

allows us to calculate the desired flux.

Now, to convert the flux into the Luminosity, we simply have to multiply by the surface area over which the flux is. This gives us the Luminosity of the Crab Nebula over the specific band as detailed above. Even though it is possible to repeat this process for every possible wavelength and filter for our object, we choose to use just one calculation to calibrate the spectra of the object. This gives us an approximation for what the total bolometric luminosity should be, while evaluating the luminosity for only one specific set of wavelengths.

Thus, we integrate over the entire spectrum with the one given luminosity value, as such:

$$L_{total} = \frac{\int_{\infty}^{\infty} f(\nu) d\nu}{\int_{\infty}^{\infty} f(\nu) * S(\nu) d\nu} * L_B, \quad (12)$$

where $f(\nu)$ is the flux distribution function.

Due to the complexity of finding an analytic form of the radiation curve of the Crab Nebula, we decided to estimate it as a black body for ease of computation. While this may not be the most accurate, it was necessary to do for the reasons listed above. In this manner, we used the equation for effective temperature

$$\log T_{eff} = c_0 + c_1(B - V) + c_2(B - V)^2 + c_3(B - V)^3. \quad (13)$$

This allows us to find the black body spectrum, given by

$$f(\nu) \propto \frac{\nu^3}{c^2} \frac{1}{\frac{h\nu}{ek_B T} - 1}. \quad (14)$$

We understand this is not the most accurate representation of the Crab Nebula, but using some assumptions, this will do for this paper. Given the resources at hand, this was the method we chose and give reasoning in our results and conclusion sections below. Here is an image of the Crab Nebula spectra, using many different filters across a multitude of orders of magnitude:

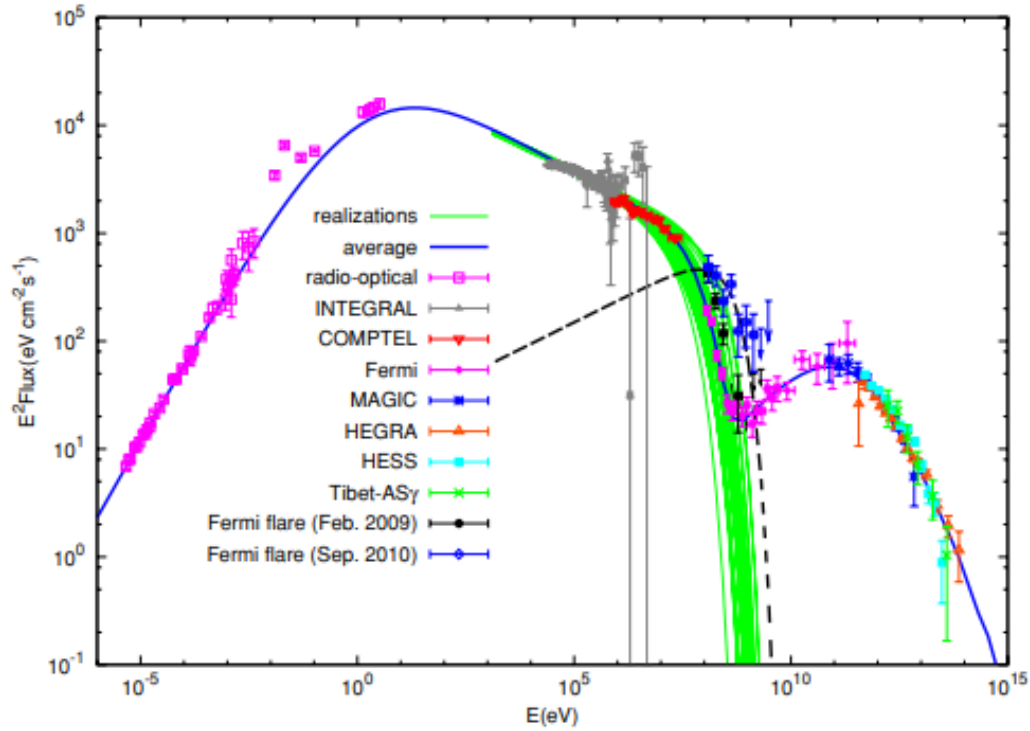


Fig. 2: True spectrum of the Crab Nebula. The spectra shows that the Crab Nebula is much more complex than a simple blackbody, and the true Luminosity would be derived using the combination of all the data gathered shown.

2.2 Data Gathering and Preparation

In this section we discuss our data gathering procedures, from collection to preparation for analysis.

2.2.1 ATNF Data

The catalog of Pulsar data we used can be found on the ATNF (Australia Telescope National Facility) website. Thanks to their Parkes Radio telescope, the ATNF provides a comprehensive list of over 2000 pulsars and various parameters (both measured and derived) that are free for viewing on their webpage or to download.

2.2.2 Database info/their sources

On their website, it is possible to choose from various parameters and display the requested data as either a plot or a table, as shown below in Figure 6.



Catalogue version: **1.68**

TABLE

PLOT

Predefined Variables [Display parameters](#)

<input type="checkbox"/> Name	<input type="checkbox"/> JName	<input type="checkbox"/> RaJ	<input type="checkbox"/> DecJ	<input type="checkbox"/> PMRA	<input type="checkbox"/> PMDec
<input type="checkbox"/> PX	<input type="checkbox"/> PosEpoch	<input type="checkbox"/> ELong	<input type="checkbox"/> ELat	<input type="checkbox"/> PMELong	<input type="checkbox"/> PMELat
<input type="checkbox"/> GL	<input type="checkbox"/> GB	<input type="checkbox"/> RaJD	<input type="checkbox"/> DecJD		
<input type="checkbox"/> P0	<input type="checkbox"/> P1	<input type="checkbox"/> F0	<input type="checkbox"/> F1	<input type="checkbox"/> F2	<input type="checkbox"/> F3
<input type="checkbox"/> PEpoch	<input type="checkbox"/> DM	<input type="checkbox"/> DM1	<input type="checkbox"/> RM	<input type="checkbox"/> W50	<input type="checkbox"/> W10
<input type="checkbox"/> Units	<input type="checkbox"/> Tau_sc	<input type="checkbox"/> S400	<input type="checkbox"/> S1400	<input type="checkbox"/> S2000	

Fig. 3: User interface for the ATNF online catalog with only certain parameter options shown.

By reading through the documentation provided, only necessary data can be displayed.

The ATNF website lists - along with the requested parameters - any error associated with the reported measurements or derived quantities and the specific source the data is from. The errors shown in the database are single integers, and represent the $+/-$ error of the final digit of the corresponding parameter displayed. The vast majority of the sources listed are academic papers which used the Parkes Radio Telescope for their findings.

The Parkes Radio Telescope is located outside Parkes, several hours inland from Sydney, Australia. It is a 64 meter telescope and one of four instruments that comprise the ATNF.

This specific telescope is responsible for the observation of over half of the total observed pulsars to date. The CSIRO also created their innovative Multi-beam Receiver with the purpose of observing 21 cm emission lines. This type of radiation is in the radio band and results from the transition between two energy levels within the ground state of Hydrogen 1, and is very pervasive throughout the entire universe. (More receiver specifications can be found on their website.)

2.2.3 Python script for data scraping

On the website, the data of each pulsar and its parameters were stored in HTML code, as to display effectively on the web page itself. For the purpose of viewing data, this method is sufficient. However, we looked to scrape the data for actual analysis with the Python library BeautifulSoup. BeautifulSoup pulls data stored in an HTML (or XTML) file and allows for access and manipulation within Python.

We quickly ran into an issue: the data (with requested parameters from the web page) is stored as text, not in a table, in the HTML file. Therefore, trying to use BeautifulSoup proved futile.

Luckily, the ATNF allows for the download of a database (.db) file with all of their data: every pulsar with all of its available parameters. After download, we forced the database to be a text (.txt) file through the terminal emulator and successfully were able to read, line by line, all of the data.

The text file was now organized as such: parameter name, parameter value, citation, and other values all in one line, as shown in Figure 4 below. An algorithm was needed to be able to parse through each line and extract only the parameter name and its corresponding value.

```

PSRJ      J0002+6216          cwp+17
RAJ       00:02:58.17        2      cwp+17
DECJ      +62:16:09.4        1      cwp+17
POSEPOCH  55806              cwp+17
F0        8.6682478274       1      cwp+17
F1        -0.448354E-12       5      cwp+17
PEPOCH    55806              cwp+17
DM        218.6              6      wcp+18
S1400     0.022              wu18
DIST_DM   6.357              ymw17
DIST_DM1  7.892              cl02
TYPE      HE[wcp+18]
ASSOC     GRS:4FGL_J0002.8+6217[fermi21],XRS:1XSPS_J000257.6+621609[wcp+18]
SURVEY    FermiBlind
@-----

```

Fig. 4: An example of 15 lines from the text file containing all of the pulsar data. Labels, respective parameters, and sources are all included.

At this point, we created an algorithm that would parse through the text file, line by line, and select the parameter name and the corresponding value.

```

47 for i in range(len(arr)-1):
48
49     j = 0
50     try:
51         while arr[i][j] != sp:
52             j += 1
53     except IndexError:
54         j = j - 1
55
56     k = 9
57     try:
58         while arr[i][k] != sp:
59             k += 1
60     except IndexError:
61         k = k - 1
62
63     if arr[i][0:j] == 'PSRJ':
64         PSRJ_arr.append(arr[i][9:k])
65     if arr[i][0:j] == 'RAJ':
66         RAJ_arr.append(arr[i][9:k])
67     if arr[i][0:j] == 'DECJ':
68         DECJ_arr.append(arr[i][9:k])
69     if arr[i][0:j] == 'POSEPOCH':
70         POSEPOCH_arr.append(arr[i][9:k])
71     if arr[i][0:j] == 'F0':
72         F0_arr.append(arr[i][9:k])
73     if arr[i][0:j] == 'F1':
74         F1_arr.append(arr[i][9:k])
75

```

Fig. 5: Snippet of code displaying parsing and array loading algorithm. (Variable and array initializations not shown.)

Figure 6 above is a snippet of code that demonstrates how the parsing algorithm works. The 'For' loop in line 47 iterates through each line of Figure 4.

Starting at the beginning of the line, with variable 'j' equaling 0 and counting up, the algorithm walks through the line until it hits a 'space' character. Now, the indices between '0' and 'j' can be sliced and stored as the parameter name. The same process is repeated but with variable 'k', iterating from the beginning of the parameter value, successfully storing those numbers to be used later for slicing. The parameter value from 'k' initial to 'k' final is loaded in to the corresponding parameter array. At the beginning of the next iteration, 'i' goes to the next line, 'j' and 'k' reset, and the process repeats.

2.2.4 Python script for data loading

Subsequent code was now needed to store the data for easy exploration and manipulation. Since not every pulsar had all identical parameters and values, it was necessary to sort the data as to not confuse data points and store them sequentially, mismatching parameter from parameter value.

To start, using the same parsing algorithm as described above, an array of unique labels is initialized and filled as to keep track of all the possible parameters as such:

```
for i in range(len(arr)-1):
    #print(arr[i])
    j = 0
    try:
        while arr[i][j] != sp:
            j += 1
    except IndexError:
        j = j - 1
    if arr[i][0:j] not in UniqueLabels_arr and arr[i][0:j] != '@-----':
        UniqueLabels_arr.append(arr[i][0:j])
```

Fig. 6: Snippet of code displaying creation of the Unique Labels array. (Variable and array initializations not shown.)

Next, it was time to load in all of the parameters and respective values as separate arrays into separate matrices for each individual pulsar.

```

for i in range(len(arr)-14):
    #print(arr[i])
    j = 0
    try:
        while arr[i][j] != sp:
            j += 1
    except IndexError:
        j = j - 1
    #print(j)
    k = 9
    try:
        while arr[i][k] != sp:
            k += 1
    except IndexError:
        k = k
    #print(k)
    l = i+1
    PulsarLabels_arr = []
    Pulsar_arr = []

    if arr[i][0:j] == 'PSRJ':
        PSRJ_arr.append(arr[i][9:k])
        PulsarLabels_arr.append(arr[i][0:j])
        Pulsar_arr.append(arr[i][9:k])
        while arr[l][0:j] != '@---' :
            m = 0
            n = 9
            try:
                while arr[l][m] != sp:
                    m += 1
            except IndexError:
                m = m - 1
            try:
                while arr[l][n] != sp:
                    n += 1
            except IndexError:
                n = n
            PulsarLabels_arr.append(arr[l][0:m])
            Pulsar_arr.append(arr[l][9:n])
            if l < len(arr)-2 :
                l += 1
            else:
                break
    if PulsarLabels_arr != [] :
        Labels_arr.append(PulsarLabels_arr)
    if Pulsar_arr != [] :
        Data_arr.append(Pulsar_arr)

```

The purpose of this code is to fill the Labels and Data matrices with arrays of labels and data points, respectively, at each index corresponding to a pulsar. This is the next step in each data manipulation, so that each index corresponds to a pulsar but in two separate arrays.

Finally, to create a data matrix that has all of the necessary information organized neatly into rows and columns, the three arrays aforementioned were needed.

```
rows = len(Data_arr)
cols = len(UniqueLabels_arr)

Data_mat = [[None for _ in range(cols)] for _ in range(rows)]

for a in range(len(Data_arr)):
    for b in range(len(UniqueLabels_arr)-1):
        for c in range(len(Data_arr[a])-1):
            if Labels_arr[a][c] == UniqueLabels_arr[b]:
                Data_mat[a][b] = Data_arr[a][c]
```

Fig. 8: Snippet of code displaying comparison of Labels and UniqueLabels arrays and the subsequent loading of the final Data matrix. (Variable and array initializations not shown.)

Figure 9 shows how the Data matrix is initialized and populated. Every row is an array with unique data from a single pulsar. Every column is an array representing a unique label. The program attempts to fill the data matrix and only fills the columns if the populated Label array and Unique Label array match for that point. The corresponding value is also populated into the data matrix, and the process is repeated until complete.

The result is a custom "search algorithm" of sorts that can pick out just the requested parameters from the entirety of the ATNF PSRCAT catalogue for a predefined list of pulsars. In the case of this paper, since we are looking to calculate the energy loss of a pulsar, we extract the spin frequency, and spin down frequency rate: 'F0' and 'F1' respectively.

As shown in Eq. 8,

$$\dot{E} = I\Omega\dot{\Omega}, \quad (15)$$

where

$$\Omega \equiv \frac{2\pi}{P} = 2\pi F. \quad (16)$$

Now, to calculate \dot{E} , we simply need to take an implicit derivative of Ω with respect to time and obtain a value for I to fully solve. We take a typical value for a canonical pulsar for its moment of inertia

$$I \approx 10^{45} \text{ gcm}^{-2} \quad (17)$$

and derive to get $\dot{\Omega}$:

$$\dot{\Omega} \equiv \frac{d\Omega}{dt} = 2\pi(1)\dot{F} = 2\pi\dot{F}. \quad (18)$$

Now, combining Eqs. 15 through 18, we can calculate \dot{E} for any pulsar within our data matrix compiled by the algorithm described above:

$$\dot{E} = 4\pi^2 I F \dot{F}. \quad (19)$$

We also take into account the error of each value obtained into separate arrays for later use in both error propagation and analysis.

2.2.5 PWNe Data

The next integral step is the accumulation of luminosity measurements for the PWNe. We started by looking for databases or catalogues similar to the one for pulsars of the ATNF but were largely unsuccessful in finding thorough and reliable databases that we could draw information from. We ended up finding a couple small catalogues that detailed certain specific parameters of PWNe, but their values had extremely large errors and provided an incomplete picture for the vast amount of PWNe that do exist. Instead, we focused on synthesizing data from a multitude of scientific sources, mostly from other academic papers.

The majority of the papers we drew information from focused on similar points. While some papers focused on describing and explaining the phenomena discovered and observed by various global surveys, others intended to prove that the correlation does indeed exist between pulsar spin down and pulsar wind nebula luminosity. Therefore, selecting these papers not only allowed us to have reliable data, but also we used them as a check for ourselves: if our data analysis and results agree with the ones from many different academic papers, we can be more sure of the methods carried out in this paper.

One of these such sources is a paper detailing the observed and measured x-ray radiation emanating from a pulsar. They detail a new survey that was conducted using two x-ray telescopes, namely the ROSAT and ASCA telescopes. The survey found almost thirty new pulsars in the universe, and many details on of the possible parameters are calculated and discussed within this paper(cite).

The main focus of the paper is to fully measure various parameters of the pulsars and any x-ray radiation produced by the spinning neutron star. By relating the energy loss of the pulsar to the x-ray luminosity observed, they claim the majority of x-ray radiation is a direct result of the co-rotating magnetosphere around the pulsar.

This is an extremely important result, as now it allows for the measurement of x-ray luminosity of the entirety of the surrounding area, including the PWNe, knowing that that a very significant portion of the x-ray radiation is a direct effect of the spinning neutron star.

3 Results

Here we discuss our various results from calculations carried out in this paper. At first, we cover the values we calculated in the first section of our methods, as described above. We discuss the mathematical formulations and analyze any error. Then, we move on to the discussion of our correlation data, and look at plots and statistical

measurements of the linear regression we carry out to look at the validity of our data and claims. We compare both the data we calculated and the data we used from various other academic paper. The comparison allows us to claim the validity of our measurements and confirm that our results are the same as the ones of various research papers in the past.

3.1 Luminosity Calculation

Using the various mathematical formulations and methods as detailed in the above methods section, we were able to calculate the spin down luminosity of the crab pulsar and the bolometric luminosity of the crab nebula that surrounds it.

The flux found for the Crab Nebula was $5.8 * 10^6$ in units of ADU and its magnitude was 13.6 using the reference star for the calculation as explained in the methods section above.

The final calculations resulted in a luminosity of

$$L_{total} = 2.0 * 10^{34} \tag{20}$$

in ergs/s which is a few orders of magnitude off of the ATNF reported value of $L_{Spindown} = 4.5 * 10^{38}$ in units of ergs/s.

This error can ber accounted for due to the propagation throughout each step of the calculation, as well as due to the background noise in the images used to calculated the flux and luminosity in the first place.

3.2 Plots and Statistics

We now can finally discuss the correlation between the Energy loss of pulsars and the observed luminosity of the pulsar wind nebulae that surround them.

In the first plot, Fig. 9, we plot the energy value we calculated from the ATNF data against the x-ray luminosity values we collected from other research papers. For the calculated energy, we multiply $F0$ and its derivative, $F1$, by the correct factors as shown in Eq. 19 and plot its logarithmic values on the x-axis. On the y-axis are the logarithmic values of Luminosity.

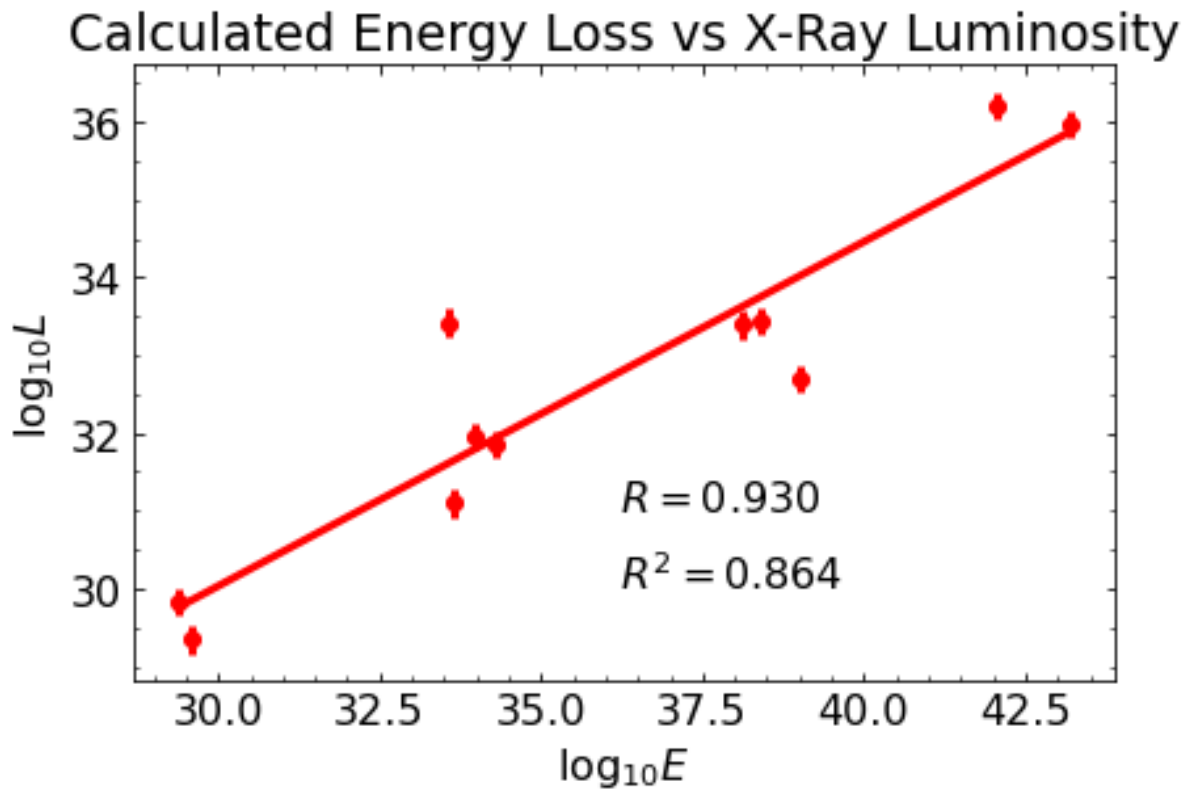


Fig. 9: Calculated Energy Loss plotted against given Luminosity in the X-ray band.

It can be clearly seen from the plot that there is a strong correlation between the two, where the R value for the linear regression is 93%. While the sample size is not very large, we are content with our linear regression values and discuss more about the validity of the sample size in our error analysis section later in this paper.

Now, in the next plot, Fig. 10, we notice a similar trend, but our parameters have changed. The calculated energy values are the exact same, as the pulsars themselves are the same. However, in this plot, we plot those values against values of bolometric luminosity.

Calculated Energy Loss vs Bolometric Luminosity

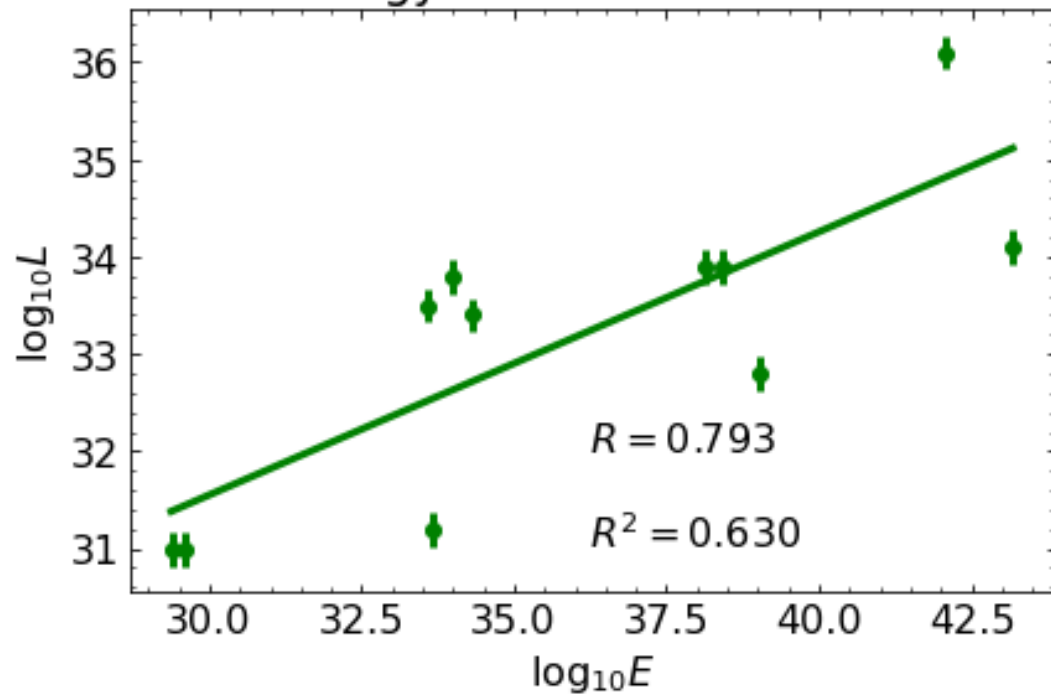
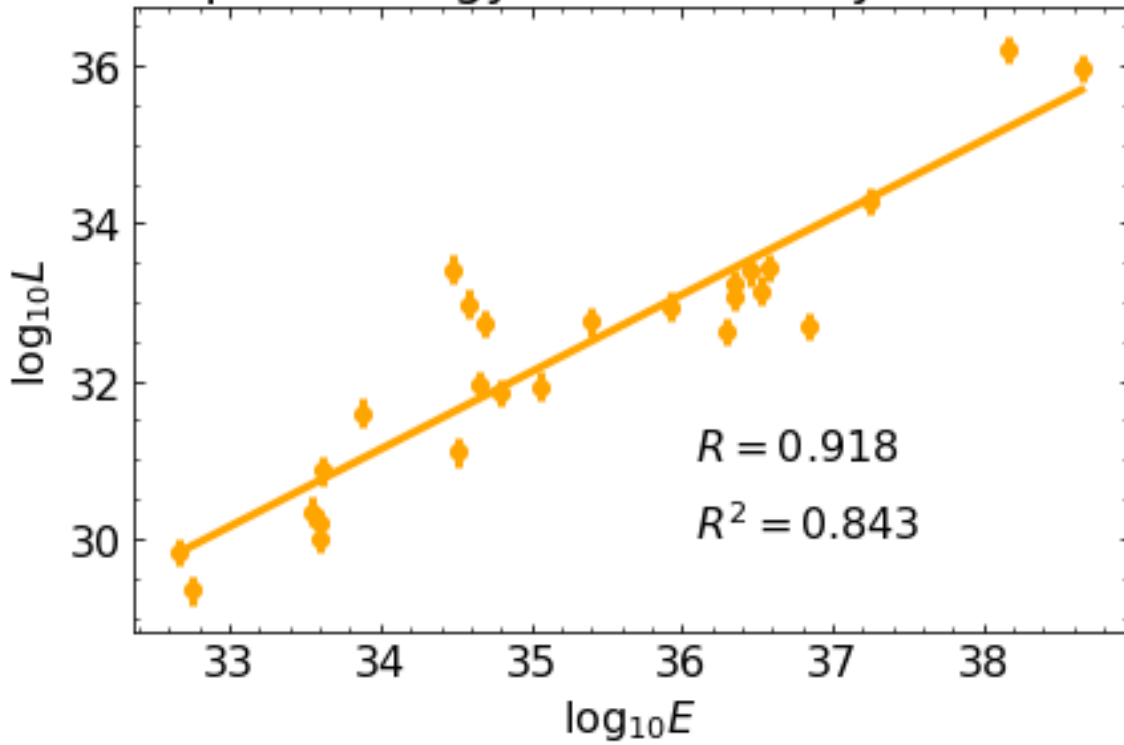


Fig. 10: Calculated Energy Loss plotted against given Luminosity over the entire electromagnetic spectrum.

Again, a clear linear relationship is visible, and a still high correlation value is reported. The relevant statistics are included in the plot but the main takeaway for the purposes of this paper is that a linear regression model fits the data quite well, and a significant majority of the data can be accounted for with a linear model.

Accepted Energy Loss vs X-Ray Luminosity



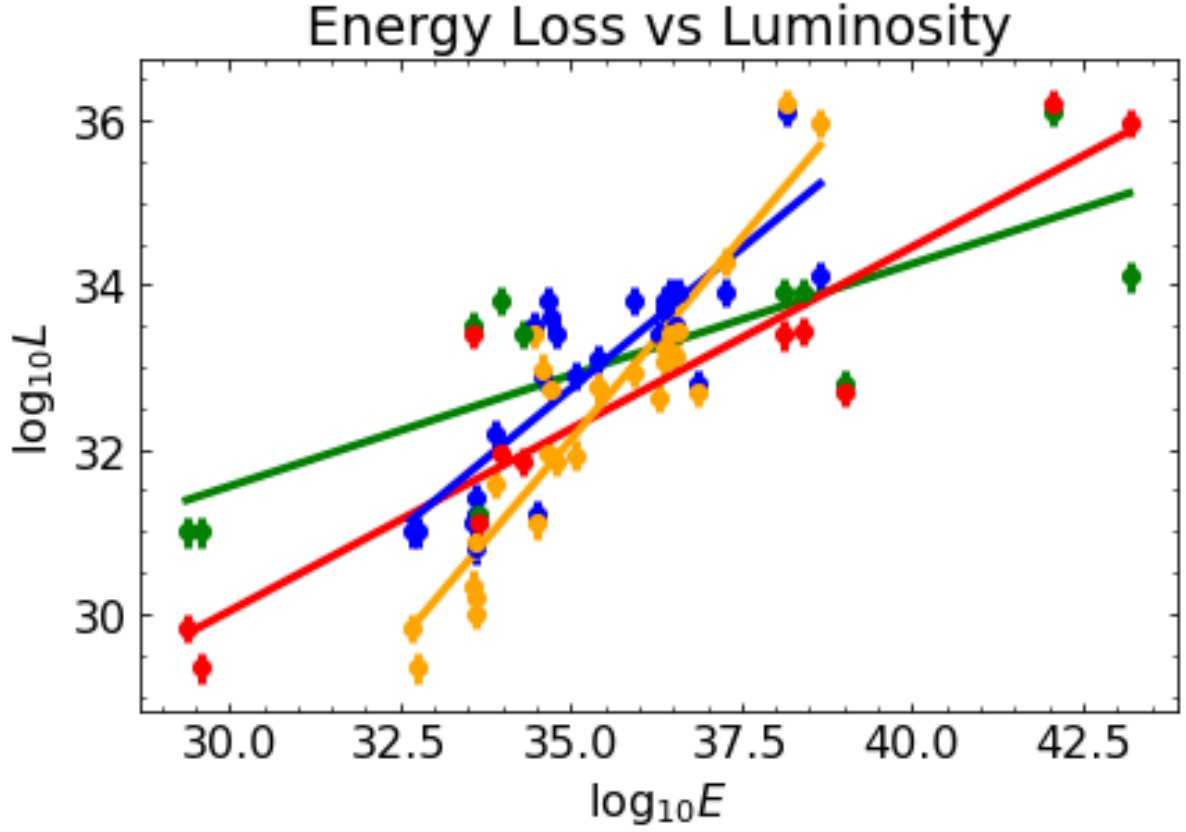


Fig. 13: Calculated Energy Loss plotted against given Luminosity in the X-ray band.

3.3 Error Analysis

The errors for the spin frequency and its derivative, the spin down frequency, are listed in the table below. The errors for each individual measurement are listed, with their source where they are found in as displayed on the ATNF's Pulsar catalogue website. The calculated Energy error column was derived in the following way:

$$\epsilon_E = \left[\frac{\epsilon_{F0}}{F0} + \frac{\epsilon_{F1}}{F1} \right] E. \quad (21)$$

As shown below, the errors of the calculated energy are so small compared to the actual values that they were omitted from the plots above. The error bars were so minuscule compared to the size of the markers or tick marks that it was futile to plot them. This is why we include this table below so that the errors may be visualized and the method with which they were calculated can be displayed as well, even though they are absent from the plots above.

F0	F1	Energy	Source
3e-10	2e-18	1.278896833e-17	lwy+16
1e-6	2e-15	5.95163110e-14	ljg+15
7e-10	8e-17	1.58184379e-15	fak15
35e-12	81e-20	3.41628126e-18	jh05
9e-11	3e-19	5.65332644e-19	hlk+04
5e-10	2e-15	2.23892920e-14	dml02
14e-12	4e-20	1.58062005e-19	hlk+04
2e-11	1e-18	5.07318561e-18	jbv+19
2e-11	9e-19	8.86800275e-18	ywml10
7e-10	5e-18	1.26479778e-16	hlk+04
2e-11	3e-18	6.05606514e-18	ymw+10

4 Conclusion

We take the time now to reflect on our methods and procedures, synthesize our results, and look to the future for possible improvements and revisions.

The methods we employed to arrive to our results proved useful and reliable, and allowed us to make claims and deduce relationships within our data. As solid as our data gathering and organization was, it remains in question how this paper may have differed had we observed and gathered all of the data ourselves. We are confident in our abilities and could have easily been able to collect all necessary data had we had the access to the correct facilities and scientific instruments. We did have access to the LCO global telescope network which proved extremely useful, but only for certain specific bands in the electromagnetic spectrum. For a more complete and diverse set of data, a more diverse set of technological equipment would be needed to observe the phenomena in the universe in other bands such as radio, x-ray, or even gamma.

The results show a very clear correlation with spin down luminosity of pulsars and the luminosity of their surrounding PWNe. Extra plots with other scientific paper's data are included as well to reinforce this point and that the scientific community is in agreement on this topic. High values of correlation and good values for R^2 for all plots prove this. The relatively low errors also reinforce this point.

We consider also how this information can be used in the future. Knowing that pulsars spin on an axis that is not aligned with their magnetic axis leads to the concept that they create a lighthouse effect that spans across the cosmos. However, sometimes the area swept by these radio jets are not in the line of sight with observations from Earth. So, while observations do reveal PWNe with relative ease, the nature of what lies inside them is unobservable. In the near future, when more and more pulsars and their PWNe become discovered and the data fits become more and more accurate with higher sample sizes, linear interpolation becomes a valid mathematical

tool in the describing of these cosmic phenomena.

5 Acknowledgments

Thank you to the University of California Santa Barbara Physics Department, Professor Philip Lubin, and Jeonghwa Kim for an extremely interesting, informative and exciting course. A further thank you to Sam Whitebook for his extremely helpful guidance throughout the duration of the course.

Lastly, a massive thank you to my co-researchers and fellow students Benjamin Riley and Hudson Powell for their help and support in the writing of this paper.

6 References

6.1 Academic Papers

<https://arxiv.org/pdf/1702.08280.pdf>
<https://iopscience.iop.org/article/10.1086/303943/fulltext/34379.text.html#dtb3>
<https://iopscience.iop.org/article/10.1088/0004-637X/694/1/12>
<https://arxiv.org/pdf/astro-ph/9708169.pdf>
<https://www.aanda.org/articles/aa/pdf/2002/21/aa1938.pdf>
<https://iopscience.iop.org/article/10.1086/425295/pdf>
<http://www.ioffe.ru/LEA/val/Lectures2015/Biblio/ch18ChengOuterGap.pdf>
https://www.isdc.unige.ch/sf2010/lectures/FA_Lecture89.pdf
<https://www.aanda.org/articles/aa/abs/2003/26/aa3605/aa3605.html>
<https://academic.oup.com/mnras/article/460/4/4011/2609171>
<https://academic.oup.com/mnras/article/446/1/857/1331802>
<https://ui.adsabs.harvard.edu/abs/2015ApJ...812...95F/abstract>
<https://iopscience.iop.org/article/10.1086/491615/meta>
<https://ui.adsabs.harvard.edu/abs/2004MNRAS.353.1311H/abstract>
<https://iopscience.iop.org/article/10.1086/339068/pdf>
<https://arxiv.org/abs/1812.04038>
<https://academic.oup.com/mnras/article/404/1/289/3101536>
<https://iopscience.iop.org/article/10.1088/2041-8205/719/2/L111/pdf>
<https://ui.adsabs.harvard.edu/abs/1998AA...333..231B>
<https://arxiv.org/pdf/astro-ph/9708169.pdf>
<https://iopscience.iop.org/article/10.1086/425295/pdf>

6.2 Websites

<http://tevcat.uchicago.edu/>

<https://lco.global/about/>

https://link.springer.com/referenceworkentry/10.1007/978-3-319-21846-5_5

<https://www.csiro.au/en/about/facilities-collections/atnf/parkes-radio-telescope>

<https://www.atnf.csiro.au/research/multibeam/lstavele/description.html>

<https://www.atnf.csiro.au/research/multibeam/lstavele/description.html>